applied sciences

MDPI

Article

New Displacement Method for Free Embedded Cantilever Walls in Sand

Murat Hamderi

Department of Civil Engineering, Turkish-German University, Istanbul 34820, Turkey; hamderi@tau.edu.tr

Abstract: In the current literature, there is no practical formula to calculate the horizontal displacement of cantilever walls. To fill this gap, in the present study, eight formulae for the estimation of wall displacement were developed based on 431 FE wall model configurations. Each formula considers factors such as the wall height, embedment depth, surcharge load, unit weight, internal friction angle, elastic modulus of the surrounding soil, and flexural rigidity of the wall. The FE model, which was used in the development of the formula, was also validated against a physical laboratory study. In addition, the outputs obtained from the formulae were compared with the results of two laboratory studies and a real site study. Finally, a parametric study was performed to estimate the influence of formula input parameters on wall displacement.

Keywords: wall displacement formula; cantilever; embedded; free walls

check for updates

Citation: Hamderi, M. New Displacement Method for Free Embedded Cantilever Walls in Sand. *Appl. Sci.* **2024**, *14*, 2802. https://doi.org/10.3390/app14072802

Academic Editor: Xinzhuang Cui

Received: 2 March 2024
Revised: 20 March 2024
Accepted: 26 March 2024
Published: 27 March 2024

1. Introduction

Free embedded cantilever walls (FECWs) are commonly employed in various forms, including contiguous pile walls (CPWs), secant pile walls (SEPWs), soldier pile walls (SOPWs), sheet pile walls (SPWs), and diaphragm walls (DWs). In CPWs, bored piles are arranged at specific intervals, while, in SEPWs, the piles overlap. SOPWs feature widely spaced piles connected with concrete, wood, or steel laggings. SPWs involve driving steel sheets into the ground at overlapping intervals. When these walls are not pinned or anchored, their stability primarily relies on the passive soil pressure on the front side, classifying them as FECWs. These walls find applications in river and shoreline protections, structural excavations, highway side walls, and cut-cover tunnels. In practice, pinned or anchored cantilever walls are designed primarily to meet the force equilibrium in the limit state. Numerous limit state approaches can be found in the existing literature, such as those proposed by Krey [1], Blum [2], Rowe [3], Brinch Hansen [4], Padfield and Mair [5], Yuan et al. [6], and Nandi and Choudhury [7]. However, compared to limit-state approaches, there are relatively few studies proposing methodologies for calculating displacements around walls supporting excavations. Peck [8] presented settlement prediction charts for the vertical settlement behind a wall due to excavation, utilizing case history data from sheet pile and soldier pile walls. Clough and O'Rourke [9] developed charts to predict lateral wall movement based on the excavation depth, bracing spacing, and flexural rigidity of the wall, employing case history data and nonlinear finite element analyses. A significant amount of case history data on wall displacements due to excavation can be found in the comprehensive study by Long [10].

Researchers proposed various methods for the design of walls under static and seismic conditions [11–17]. Singh and Chatterjee [13] focused on free embedded cantilever walls (FECWs) and incorporated parameters such as the internal friction angle, wall–soil interface friction angle, and surcharge load. Their method can be classified as displacement-based, as it utilizes displacement-based earth coefficients proposed by Zhang et al. [18]. Nandi and Choudhury [19] calculated the displacement-dependent earth pressure around FECWs. They also determined the bending moment distribution and ground settlement profile behind the wall, comparing the results with those obtained from PLAXIS 2D.

In the current literature, there is no practical formula to calculate the horizontal displacement of cantilever walls. To fill this gap in the literature, in the present study, eight formulae were developed to estimate the horizontal displacement of free embedded cantilever walls. These formulae were based on 431 finite element (FE) wall configurations, considering parameters such as the wall height, flexural rigidity, embedment length, surcharge load, soil modulus, internal and interface friction angles, and unit weight of the soil. The FE software MIDAS GTS NX (ver. 2019-1.1) was utilized to model and analyze the 431 wall configurations. The methodology employed in generating these wall configurations is detailed in Section S1. The formulae cover nominal wall heights of 1 m, 2 m, 3 m, 4 m, 5 m, 6 m, 7 m, and 8 m. The FE model was validated against laboratory studies conducted by Chavda et al. [20] and Basha et al. [21], and the formulae were also applied to an on-site wall test conducted by Li and Lehane [22] and a laboratory study by Bica and Clayton [23].

2. Materials and Methods

2.1. Statement of the Problem

During the initial design phase of an embedded wall, it is preferable to minimize the use of anchors and pins. In cases where the goal is to avoid these additional supports entirely, accurate estimation of wall displacement becomes crucial since the free-standing body of the free embedded cantilever wall (FECW) relies solely on passive pressure. Figure 1 illustrates an example of a FECW.

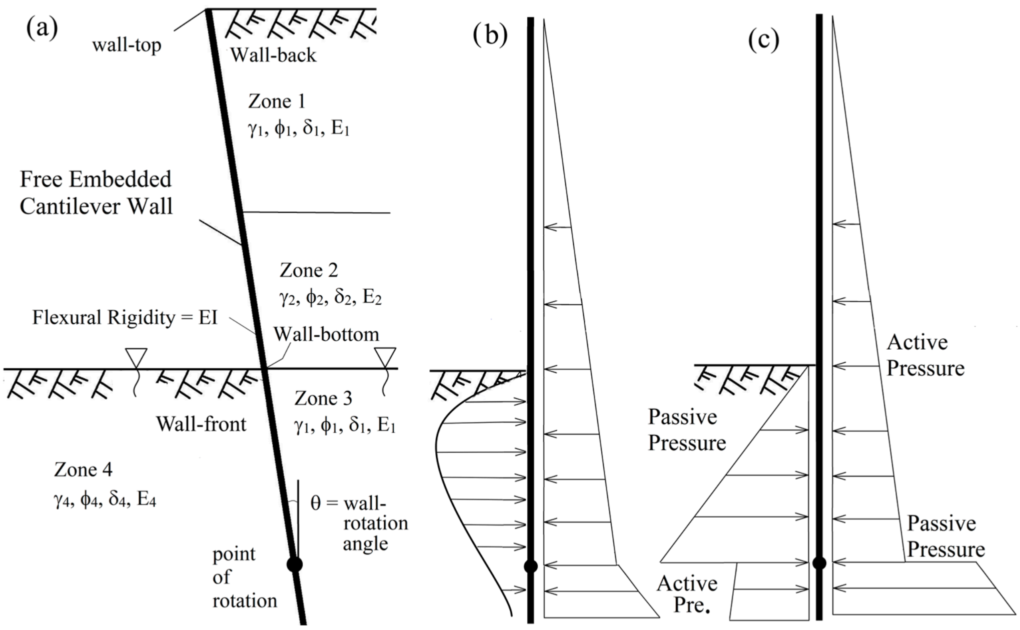

Figure 1. (**a**) An illustration of FECW along with other parameters, (**b**) expected distribution around the wall (Padfield and Mair [5]), and (**c**) the simplified pressure distribution around the wall.

Currently, displacement analyses are typically performed using finite element (FE) methods. However, FE methods can be time-consuming and expensive compared to manual calculations. The FE-based formulae presented in this study aim to simplify the wall-type selection process during the initial design phase. These formulae are specifically developed for estimating horizontal displacements at the "wall-top" and "wall-bottom" locations, as indicated in Figure 1.

Around the FECW, two distinct zones are defined: the "wall-back" and "wall-front" zones. The wall-front zone refers to the retaining zone where passive earth pressure develops above the point of rotation. The distribution of passive pressure in this zone typically follows a parabolic shape (as shown in Figure 1b, based on Padfield and Mair [5]).

However, for practical purposes, this distribution is often simplified to a triangular shape (as depicted in Figure 1c). In the wall-back zone, the active pressure distribution predominates above the point of rotation (as shown in Figure 1b,c). Below the point of rotation, the pressure state lies somewhere between active and passive. For simplicity in practice, the active and passive pressure are inverted below the point of rotation (as illustrated in Figure 1c).

The wall-back zone is further subdivided into three zones, Zone 1, Zone 2, and Zone 3, while the wall-front zone is referred as Zone 4. Each of these zones is characterized by specific components, including soil unit weight (γ), soil friction angle (ϕ), wall–soil interface friction angle (δ), and soil modulus (E). The corresponding subscripts 1, 2, 3, and 4 are added to denote the components specific to each zone. The flexural rigidity of the wall (EI) is also taken into account. It is assumed that the water table is located at the wall-bottom (Figure 1).

2.2. Validation of the FE Model with Chavda et al. [20]

Chavda et al. [20] conducted laboratory tests using a sand-filled box, where polyacetal rods were employed to retain the soil (as depicted in Figure 2). The length of each rod was 405 mm, and they varied in diameter between 8 mm, 10 mm, and 12 mm, depending on the specific test configuration. The rods were tightly aligned with no gaps between them. The relative density of the sand was adjusted to 15%, 35%, 65%, and 85% across different test configurations.

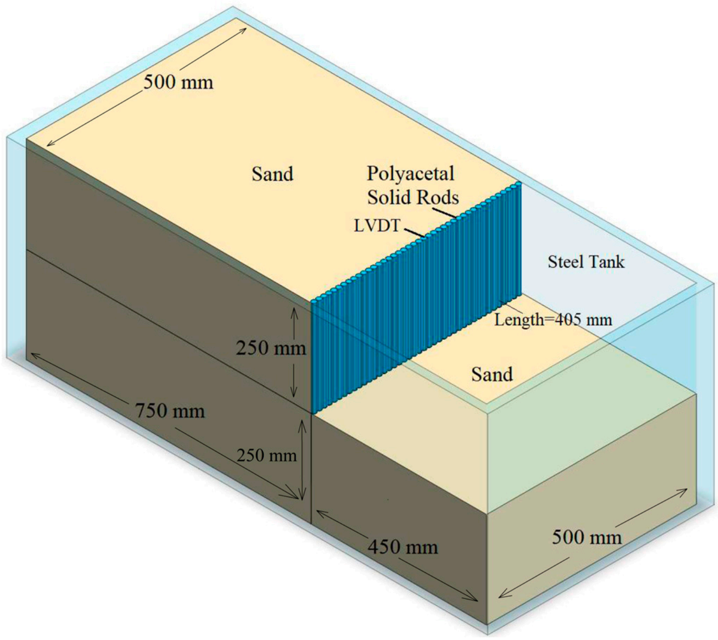

Figure 2. The illustration of the laboratory test by Chavda et al. [20].

In each test, a 50 mm section of the sand was excavated, and horizontal displacement readings were obtained using a linear variable differential transformer (LVDT) positioned at the top of the middle rod. To validate the test results, Chavda et al., 2017 performed three-dimensional (3D) finite element (FE) modeling using the PLAXIS-3D software. They compared the results obtained from the tests with the corresponding FE results for three configurations, wherein the rod diameters were 8 mm, 10 mm, and 12 mm, respectively.

In this study, a two-dimensional (2D) finite element (FE) mesh of the validation model was created using the MIDAS GTS NX (ver. 2019-1.1) software. Figure 3 presents the details of the mesh configuration. The longitudinal dimensions of the actual test conducted by Chavda et al. [20] were adopted, along with other relevant dimensions. In the FE program, the polyacetal rods were modeled as beam elements, and the flexural stiffness (EI) was automatically calculated by the software for a depth of 1 m.

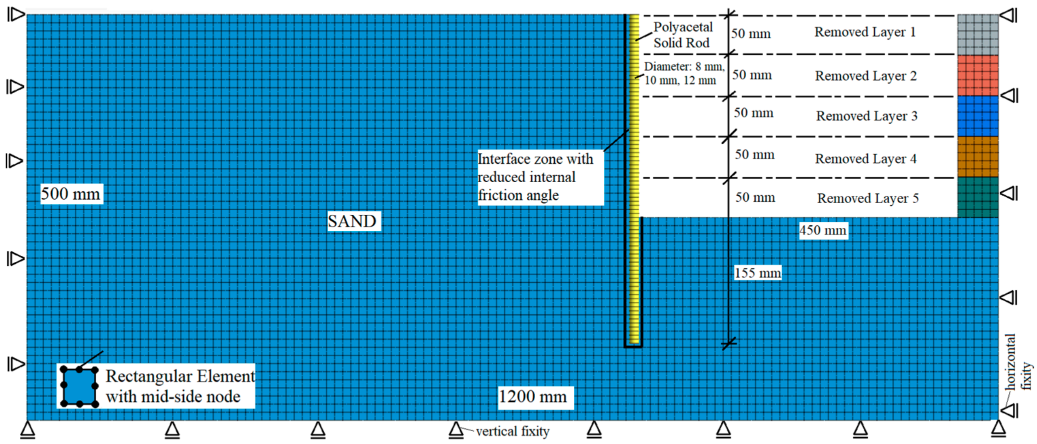

Figure 3. The 2D FE mesh of the validation with Chavda et al. [20] in MIDAS GTS NX program.

Staged construction was employed in the FE model analyses. In the first construction step, the initial geological stresses were calculated, and the displacements were set to zero. In the second step, the beam (wall) was activated, and the displacements were once again set to zero. In subsequent stages, a layer of soil with a height of 50 mm was removed, as shown in Figure 3. This process was repeated five times.

In the reference study, the internal friction of the sand was determined through direct shear tests, while the soil modulus was estimated from a plate load test conducted in the sand box. Various relative density levels were examined, namely, 15%, 35%, 65%, and 85%. In this study, the test performed in the sand box at a relative density of 35% was incorporated. The sand with a relative density of 35% had a unit weight (γ) of 14.72 kN/m^3 and an internal friction angle (ϕ) of 30°. The soil modulus at 35% relative density, which was determined based on the plate load test, was relatively small, namely, 1365 kPa. In the reference study, the soil modulus value was estimated as 3000 kPa for the sand with an 85% relative density. It is worth noting that the soil modulus of clean sand tends to increase with increasing confining pressure. Considering the relatively small confining pressure developing in the test box, the range of soil modulus values falls within a reasonable range.

The soil in the FE model was simulated using the Mohr–Coulomb soil model. In a typical FE mesh, it is important to have a sufficiently small mesh size in the area of interest. In this validation study, the critical area was around the polyacetal rods with a mean diameter of 10 mm, which were modeled as beam elements. To ensure continuity around the rods, similar-sized mesh elements with mid-side nodes (10 mm × 10 mm quadrilaterals) were employed. The rest of the model was also meshed with 10 mm × 10 mm elements, although a coarser mesh would have been sufficient (as shown in Figure 3).

The 2D mesh included horizontal fixities on the sides and vertical fixities at the bottom, as depicted in Figure 3. The analysis condition of the model was assumed to be plane-strain, meaning that no strains develop in the out-of-plane direction. Although the model is 2D, the MIDAS GTS NX program handles the stiffness matrix in three dimensions. Therefore, for compatibility purposes, fixities were included in the out-of-plane direction (Z direction) at the nodal points. The unit weight and modulus of elasticity of the polyacetal rods were reported to be 14.55 kN/m^3 and 3,000,000 kPa, respectively. All input parameters reported in the reference study were adopted "as is" except for the internal friction of the sand, which was set to 30.75° instead of 30°. This adjustment was made because the 2D FE system collapsed at the last excavation stage when the internal friction angle was set to 30° (Table 1). However, Chavda et al. [20] was able to achieve reasonably close results using a 3D FE model with an internal friction angle of 30°. The small difference in friction angles is considered reasonable since the reference study used a 3D model. To the best of the author's knowledge, 3D models tend to yield slightly better results compared to 2D models. Additionally, small variations in the friction angle were extremely critical in this study because the system was close to failure after the last excavation step. Around the wall, the soil–wall interface friction angle was set to 60% of the internal friction angle (Figure 3). The relationship between the internal friction angle (ϕ) and the soil–wall interface friction angle (ϕ_{int}) can be expressed using the following equation:

$$\tan \phi_{int} / \tan \phi = 0.6 \quad (1)$$

Table 1. The material input parameters of the FE validation in comparison with the actual laboratory test performed by Chavda et al. [20].

Parameters	Chavda et al. [20]	This Study (Midas GTS NX)
Unit weight of sand (kN/m^3)	14.72	14.72
Internal friction of sand (°)	30	30.75
Interface friction angle (°)	19.08	19.64
Poisson's ratio of sand	0.333	0.333
Mod. of elasticity of sand (kPa)	1365	1365
Mod. of elasticity of polyacetal rods (kPa)	3,000,000	3,000,000
Unit weight of rods (kN/m^3)	14.55	14.55
Poisson's ratio of rods	0.35	0.35

Based on Figure 4, the displacements obtained from the MIDAS GTS NX program for rod diameters of 8 mm, 10 mm, and 12 mm were compared with the test and PLAXIS 3D analysis results conducted by Chavda et al. [20]. The comparison shows that the results from the MIDAS GTS NX program are reasonably close to the experimental and PLAXIS 3D analysis results.

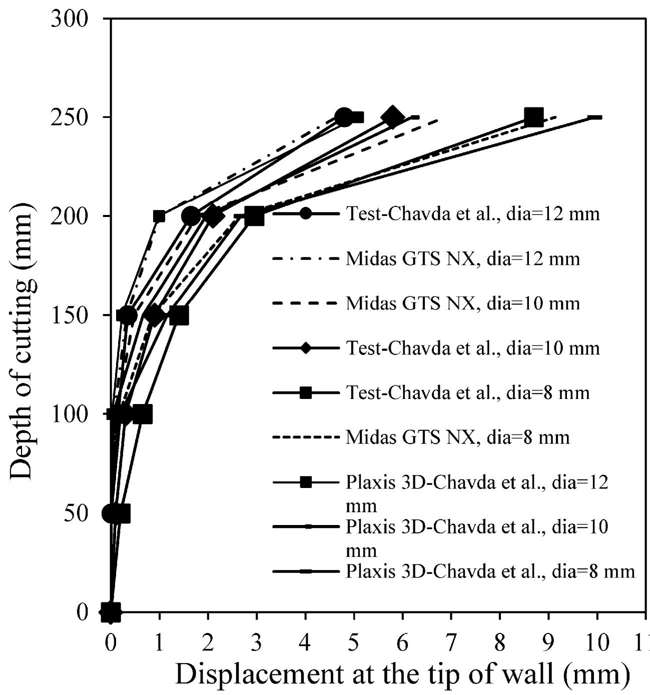

Figure 4. The plots of wall displacements from 3 sources: Midas GTS NX analyses (this study), the laboratory tests (Chavda et al. [20]), and Plaxis 3D analyses (Chavda et al. [20]).

2.3. Validation of the FE Model with Basha et al. [21]

Another example of a test on the displacement characteristics of the cantilever walls has recently been performed by Basha et al. [21], who measured the displacement of a cantilever wall embedded in sand contained by a steel-reinforced tank 3300 mm in length, 2000 mm in height, and 300 mm in width (Figure 5a). The cantilever wall consisted of 6 reinforced concrete piles 60 mm in diameter and 1500 mm in length. The piles overlapped with each other and were centered at a distance of 48 mm (Figure 5b). The tests were performed at two different relative densities for sand, namely, 60% and 80%. In each test, a uniform surcharge pressure applied on the surface behind the wall (4 kPa, 8 kPa, or 12 kPa). In each test, the sand in the front of the wall was excavated at a maximum depth of 750 mm. The minimum embedment depth of the wall was 750 mm. The horizontal wall displacement was recorded at 250 mm, 500 mm, and 750 mm excavation depths.

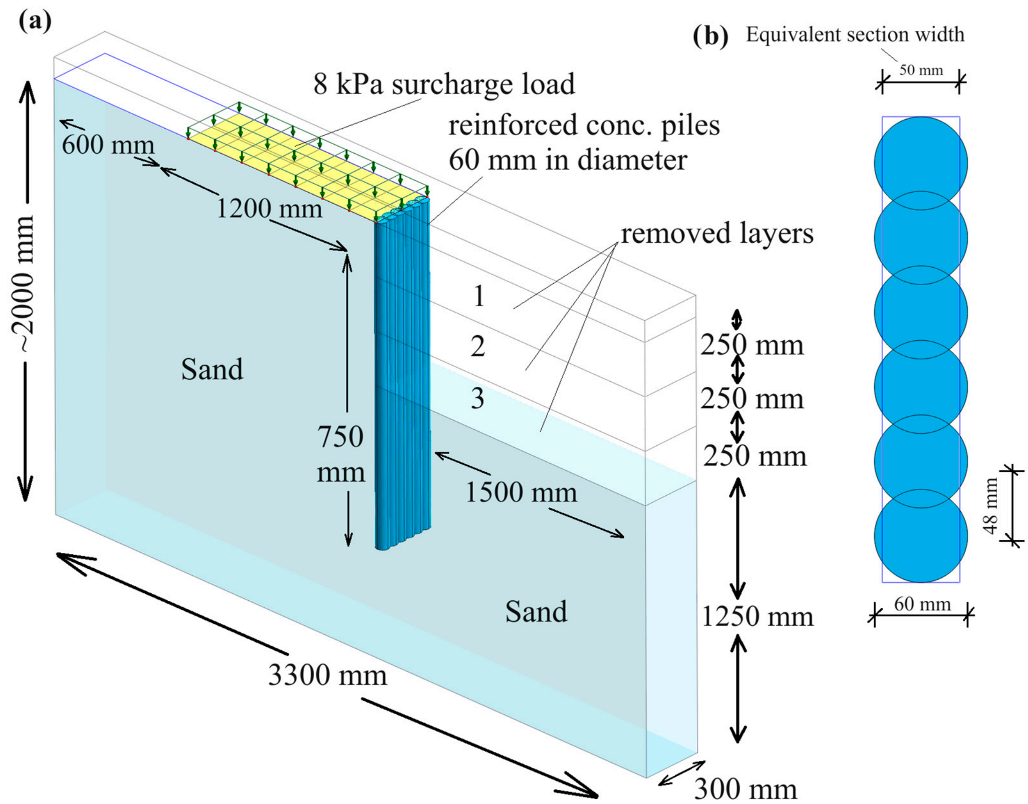

Figure 5. (**a**) The illustration of the laboratory test by Basha et al. [21], and (**b**) the alignment of piles in the cantilever wall.

The test configuration with 8 kPa surcharge pressure and 80% relative density was applied to the FE model. The FE configuration of Basha et al.'s test was similar to that of test by Chavda [20]. The details of the mesh are illustrated in Figure 6.

The material properties used in the finite element model are presented in Table 2, along with the ones provided in the reference study. The two most critical parameters for the wall displacement are the internal friction angle and the soil modulus. The maximum value given in the reference study for the internal friction angle (42.9°) was adopted, due to the fact that the sand was in dense state and the horizontal displacement developed in the tests did not indicate a condition in which the sand behind the wall was close to the failure. Janbu offered an equation where the initial soil modulus is an exponential function of confining pressure σ_3 (Equation (2)) [24]. Exponent "n" is typically given as 0.5 for dense sand (Duncan and Chang [25]).

$$E_i \propto (\sigma_3)^n \tag{2}$$

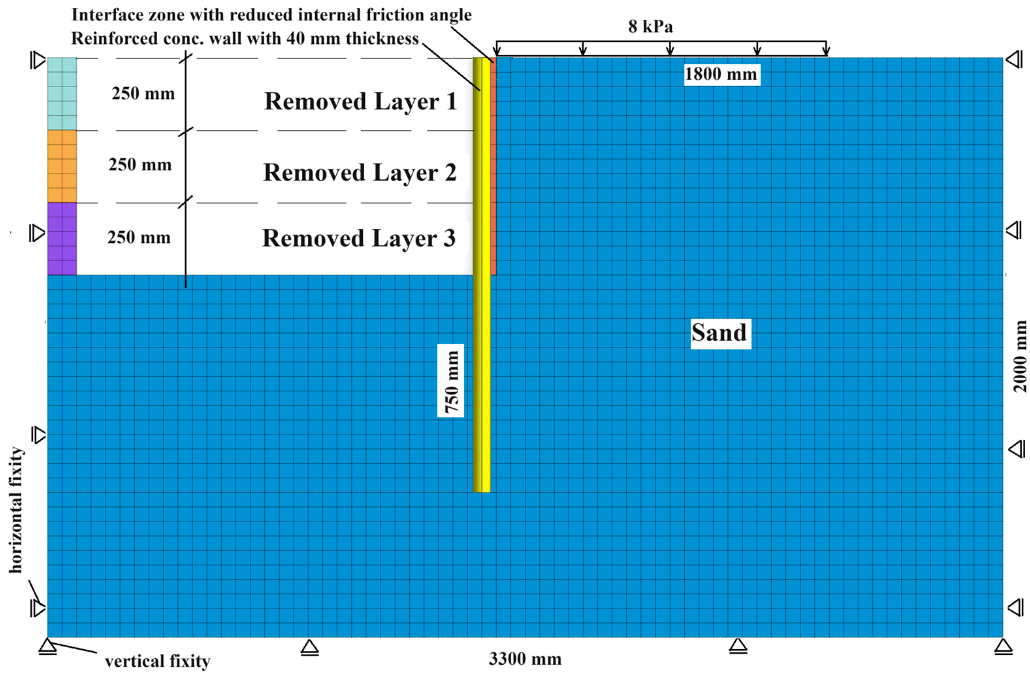

Figure 6. The 2D FE mesh of the validation with Basha et al., 2023 in MIDAS GTS NX program.

Chavda et al. [20] estimated the soil modulus of the sand with 85% relative density as 3000 kPa. Assuming that the unit weights of dense sand at both tests were more or less equal, the mean wall backfill depth can represent the confining pressure. The mean wall backfill depth in the test by Chavda et al. [20] was 250 mm/2 = 125 mm. The same height was 750 mm/2 = 375 mm for the test by Basha et al. [21]. In this case, using Equation (2), the corresponding soil modulus for the test by Basha et al. will be 3000 kPa × (375 mm/ 125 mm)0.5 ≈ 5200 kPa (Table 2). The pile-wall was modelled as a beam element with an equivalent thickness of 50 mm (Figure 5b).

Table 2. The material input parameters of the FE validation in comparison with the actual laboratory test performed by Basha et al. [21].

Parameters	Basha et al. [21]	This Study (Midas GTS NX)
Unit weight of sand (kN/m^3)	17.62	17.62
Internal friction of sand (°)	30–42.9	42.9
Interface friction angle (°)	-	29
Poisson’s ratio of sand	-	0.333
Mod. of elasticity of sand (kPa)	-	5200
Mod. of elasticity of pile walls (GPa)	-	30
Unit weight of pile walls (kN/m^3)	-	24
Poisson’s ratio of rods	-	0.2

The displacements obtained from the MIDAS GTS NX program and the test performed by Basha et al. [21] were compared in Figure 7. The results from two sources came out to be very similar. The agreement between the numerical analysis and the experimental results provides confidence in the accuracy and reliability of the FE model for simulating the behavior of the free embedded cantilever walls.

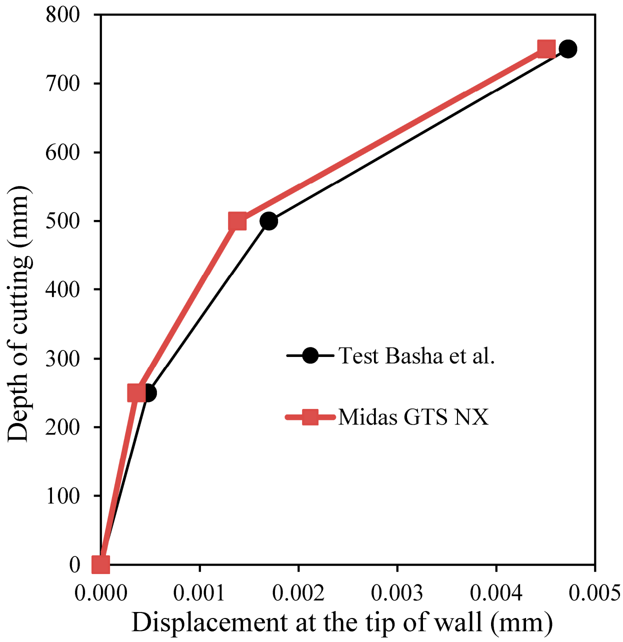

Figure 7. The plots of wall displacements from 2 sources: Midas GTS NX analyses (this study), and the laboratory tests by Basha et al. [21].

2.4. The Setup of FE Model for Formula Derivation

The equations for FECWs were derived utilizing 431 FE model configurations. The overall mesh configuration varied with respect to the wall size. A representative mesh configuration is presented in Figure 8. The heights (H) of the walls ranged from 1 to 8 m, and, for each wall height, a common mesh was used as a base from which different sub-configurations could be derived. These meshes are presented in Section S2, Figures S1–S8. The embedment depth (d) varied from 0.6 H to 1.2 H. For example, to derive different embedment depths, the length of the beam was changed in the common mesh. Further various sub-configurations could be derived by only changing the soil modulus and unit weight and internal friction angle of the common mesh.

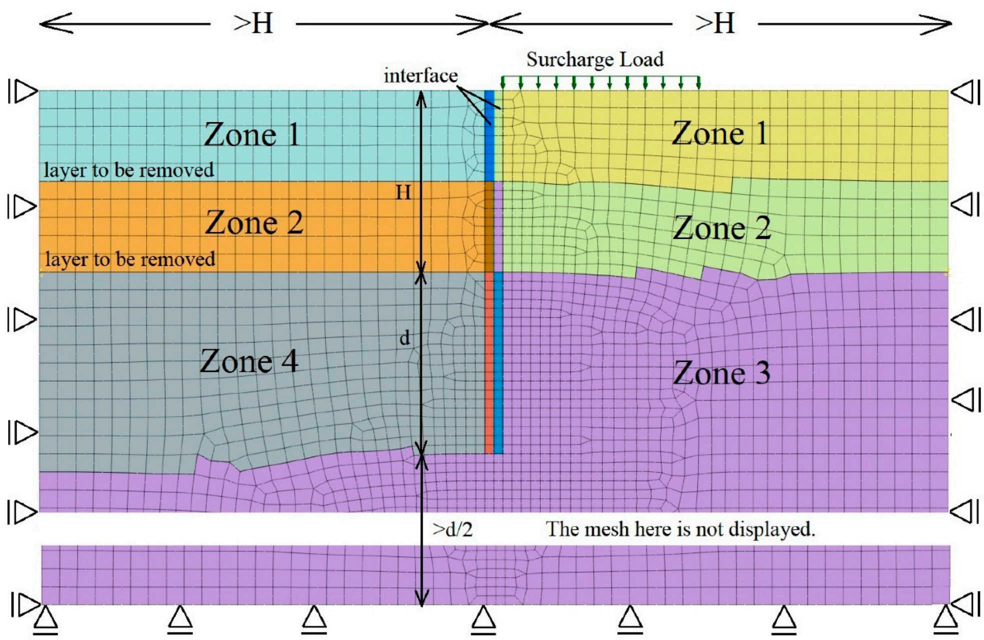

Figure 8. A representative mesh for all configurations.

The mesh size was determined based on a convergence optimization procedure. The details of this procedure are given in Section S3. In all mesh configurations, quadratic mesh elements with mid-side nodes were used and the size of the mesh element was 50 mm around the beam, whereas it was between 100 and 250 mm on the sides. During the analyses, staged construction was adopted. After the generation of initial stresses, 0.5 m- to 2 m-thick layers were removed and the displacements on the wall beams were recorded.

Table 3 summarizes the parameter ranges used in the 431 finite element (FE) model configurations for the analysis of free embedded cantilever walls (FECWs). These parameters, along with their variations, are also visually presented in Figure 1 and Section S1. The friction angles (ϕ_1, ϕ_2, ϕ_3, and ϕ_4) were varied between 25° and 42°. The wall–soil interface friction angles were set to 0.6 times the corresponding soil friction angle ($0.6\phi_1$, $0.6\phi_2$, $0.6\phi_3$, and $0.6\phi_4$). The surcharge load intensity ranged from 0 kN/m to   kN/m. The unit weight of the soil and the soil modulus varied between 16–24 kN/m^3 and 10–250 MPa, respectively. The wall height ranged from 1 m to 8 m. The flexural rigidity of the wall, represented by the product of the bending modulus and the moment of inertia (EI), ranged from 2500 kN·m^2 to 20,000,000 kN·m^2. This range includes different types of walls such as soldier piles, sheet piles, contiguous piles, secant piles, and concrete diaphragm walls (Long et al. [10]). These parameter ranges were utilized to cover a wide spectrum of practical scenarios and to study the behavior of FECWs under various conditions.

Table 3. The parameter range in 431 FE model configurations.

Description	Symbol	Values	Unit
Internal friction angle of soil	ϕ_1, ϕ_2, ϕ_3, ϕ_4	25, 28, 30, 35, 40, 42	°
Wall–soil interface friction angle	δ_1, δ_2, δ_3, δ_4	$0.6\phi_1$, $0.6\phi_2$, $0.6\phi_3$, $0.6\phi_4$	°
Unit weight of soil	γ_1, γ_2, γ_3, γ_4	16, 18, 20, 22, 24	kN/m^3
Line load	L	0, 5, 10, 15	kN/m
Soil modulus	E_1, E_2, E_3, E_4	10, 25, 50, 75, 100, 150, 250	MPa
Wall height	H	1, 2, 3, 4, 5, 6, 7, 8	m
Wall embedment depth	d	0.6H, 0.7H, 0.8H, H, 1.2H	m
Flexural rigidity (per 1 length)	EI	2.5, 20, 39, 312.5, 2500, 8437.5, 20,000	1000 KNm^2

2.5. Formula Description

The equations were derived using the Solver function in Excel® 2007 by implementing multivariable regression analyses. The details of the derivation steps are presented in Section S4. The same procedure has also been used to derive pile settlement and axial pile load distribution formulae in the earlier studies of the author (Hamderi [26–28]). The wall-top (dispwall-top) and wall-bottom (dispwall-bottom) displacements can be estimated by the following equation:

$$disp_{wall-top}\ or\ disp_{wall-bottom} = a_H.(d)^{b_H}.(\gamma_1)^{c_H}.(\gamma_2)^{d_H}.(\gamma_3)^{e_H}.(\gamma_4)^{f_H}\left(\frac{E_1}{50000}\right)^{g_H}.\left(\frac{E_2}{50000}\right)^{h_H}.\left(\frac{E_3}{50000}\right)^{i_H}.$$
$$\left(\frac{E_4}{50000}\right)^{j_H}.\left(\frac{5+L}{5}\right)^{k_H}.\left(\frac{\phi_1}{35}\right)^{l_H}.\left(\frac{\phi_2}{35}\right)^{m_H}.\left(\frac{\phi_3}{35}\right)^{n_H}.\left(\frac{\phi_4}{35}\right)^{o_H}.\left(\frac{EI}{2500000}\right)^{p_H} \quad (3)$$

a_H, b_H, c_H, d_H, e_H, f_H, g_H, and h_H are the fitting coefficients (Table 4). The coefficients should be chosen from the table based on the nominal wall height H. The table contains coefficients for 8 different nominal wall heights. If the actual wall height falls between these values, a linear interpolation should be applied. Additionally, Table 4 provides two sets of coefficients for each height, specifically for the wall-top and the wall-bottom (see also Figure 1). If ground water is to be defined at the wall-bottom level, the values of γ_3 and γ_4 should correspond to effective unit weights.

Table 4. The fitting coefficients of the displacement equation.

H	Location	a_H	b_H	c_H	d_H	e_H	f_H	g_H	h_H
1	*top*	0.000751	−3.681073	0.874446	0.037018	−0.167765	−1.132080	−0.114422	−0.131473
	bottom	0.000297	−0.195714	0.180479	0.130834	−0.190758	−0.294169	0.178088	0.161811
2	*top*	0.004238	−4.627014	1.580239	0.263080	−0.509416	−0.654539	−0.132988	−0.188240
	bottom	0.001633	−3.619452	0.743411	0.871635	−0.065880	−0.962452	−0.050031	−0.046643
3	*top*	0.006848	−3.778154	1.668278	0.462059	−0.339251	−0.657427	−0.012539	−0.079034
	bottom	0.003249	−3.076464	1.394232	0.418696	−0.372756	−0.527647	−0.046927	−0.057883
4	*top*	0.161552	−3.821589	1.442561	0.322154	−0.299284	−0.805481	−0.010489	−0.028511
	bottom	0.005441	−2.886010	1.518921	0.626422	−0.338559	−0.652622	−0.001065	−0.028182
5	*top*	1.983635	−4.123180	1.037838	0.556425	−0.427069	−0.763103	−0.107463	−0.158713
	bottom	0.008859	−3.220532	1.405312	1.151392	−0.394873	−0.645440	−0.089302	−0.096639
6	*top*	0.550254	−3.221843	1.077035	0.455111	−0.377468	−0.469539	−0.056571	−0.045417
	bottom	0.228042	−2.574661	0.776196	0.391554	−0.509505	−0.309564	−0.046029	−0.079646
7	*top*	0.963301	−2.774572	1.278889	0.223251	−0.283519	−0.673382	−0.018681	−0.032146
	bottom	0.492712	−2.435834	1.139236	0.153125	−0.427222	−0.597964	−0.058049	−0.072019
8	*top*	0.400225	−2.114759	1.150739	0.221914	−0.256674	−0.497471	−0.021692	−0.036475
	bottom	0.270818	−2.457951	1.231097	0.278250	−0.354510	−0.477210	−0.061002	−0.058278
H	**Location**	i_H	j_H	k_H	l_H	m_H	n_H	o_H	p_H
1	*top*	−0.299084	−0.481806	1.786120	−1.182829	−1.983436	−1.733577	−2.522970	−0.116770
	bottom	−0.151804	−1.119914	1.400395	−1.288249	−1.307075	−1.371029	−0.417511	−0.009546
2	*top*	−0.462954	−0.239061	0.756286	−1.062495	−2.692397	−0.811299	−2.836539	−0.090781
	bottom	−0.463731	−0.424490	0.543194	−0.489362	−2.422801	−1.139685	−2.310535	−0.012753
3	*top*	−0.545990	−0.356649	0.622400	−1.306125	−2.350820	−1.767801	−2.192104	−0.086227
	bottom	−0.385057	−0.513123	0.569747	−1.191116	−2.104118	−1.767939	−1.933426	−0.038697
4	*top*	−0.279600	−0.650152	0.191945	−1.222934	−2.289122	−1.566682	−1.807698	−0.148619
	bottom	0.090577	−1.084779	0.158342	−1.113048	−1.959488	−1.501961	−1.399658	−0.065249
5	*top*	−0.339372	−0.362099	0.449278	−1.616237	−2.572126	−1.330509	−1.690376	−0.211811
	bottom	−0.267200	−0.548373	0.368879	−1.215475	−2.167198	−1.432462	−1.340262	−0.026833
6	*top*	−0.398372	−0.307263	0.324906	−1.249293	−2.324040	−1.008289	−1.667962	−0.118045
	bottom	−0.274219	−0.498080	0.300670	−1.176806	−2.056203	−1.092668	−1.452922	−0.049613
7	*top*	−0.203063	−0.595961	0.246227	−1.155012	−2.053339	−1.021156	−1.658725	−0.145911
	bottom	−1.628508	−0.751516	0.245908	−1.214304	−2.165633	−0.932246	−1.617343	−0.036433
8	*top*	−0.256610	−0.232423	0.208726	−1.098686	−1.790088	−1.214952	−1.560461	−0.196323
	bottom	−0.232312	−0.448886	0.527909	−1.125850	−1.799890	−1.380776	−1.607421	−0.081811

3. Results and Discussion

3.1. Application of the Formula to the On-Site Test by Li and Lehane [22]

Li and Lehane [22] reported a well-instrumented, full-scale, cantilever contiguous pile test at the University of Western Australia in Perth. The piles used in the test were continuous flight auger (CFA) piles with a diameter of 0.225 m and a length of 3.7 m. The spacing between the piles ranged from 0.3 m to 0.5 m. The geological composition at the site consisted of a 5 m- to 7 m-thick layer of siliceous spearwood sand, underlain by Tama Limestone (Li and Lehane [22]). All piles were embedded within the sand deposit. During the test, the displacement of the wall was measured at different depths of excavation. In this section, the wall displacement will be calculated using Equation (2) for excavation depths of 1.2 m, 1.7 m, and 2.2 m. A summary of the input and output parameters is provided in Table 5.

Table 5. Summary of wall displacement predictions using Equation (3) (input data from Li and Lehane [22]).

1	2	3	4	5	6	7	8	9	10
H	d	For. used	γ_1	γ_2	γ_3	γ_4	E_1	E_2	E_3
m			kN/m^3				kPa		
1.2	2.5	H = 1, H = 2	17	17	17	17	2250	6750	18,375
1.7	2	H = 1, H = 2	17	17	17	17	3375	9750	20,250
2.2	1.5	H = 2, H = 3	17	17	17	17	4125	12375	22,125
11	12	13	14	15	16	17	18	19	20
E_4	L	ϕ_1	ϕ_2	ϕ_3	ϕ_4	EI	disp (wall-top)	disp (wall-bottom)	rotation
kPa	kN/m		o			kN·m^2	10^{-3} m		Rad
18,375	0	43	43	43	43	9435	0.2	0.1	0.0001
20,250	0	43	43	43	43	9435	0.7	0.5	0.0001
22,125	0	43	43	43	43	9435	13.8	4.2	0.0044

The calculations steps of Table 5 are as follows:

1. The initial column comprises the specific wall height, Ha (or frontal excavation depth), under consideration.
2. In the second column, the embedment depths are calculated by subtracting the first column from the full pile length, 3.7 m.
3. If none of the actual wall heights correspond to any of the nominal wall heights (1, 2, 3, 4, 5, 6, 7, and 8 m), interpolation is performed using two formulae associated with the nearest nominal wall heights. The third column indicates the wall heights used in these formulae.
4. The fourth, fifth, sixth, and seventh columns represent the unit weights of the wall-back and wall-front zones, respectively. These values are directly taken from the reference study conducted by Li and Lehane [22].
5. The eighth, ninth, tenth, and eleventh columns indicate the soil moduli of the wall-back and wall-front zones. The distribution of the soil modulus in sand (Li and Lehane [22]) was calculated by multiplying the CPT tip resistance (q_c) by 3 (Bowles [29]). The distributions of q_c, E1, E2, E3, and E4 with respect to depth are presented in Figure 9. The moduli are assigned to zones as depicted in Figure 10.

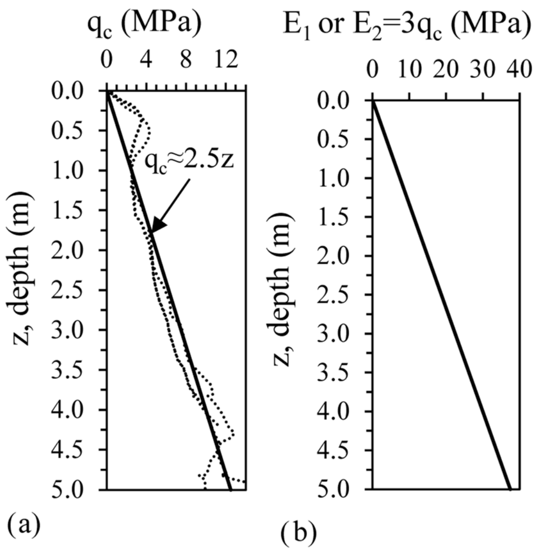

Figure 9. The distributions of (**a**) q_c, and (**b**) E1, E2, E3, and E4 with depth (q_c data from Li and Lehane [22]).

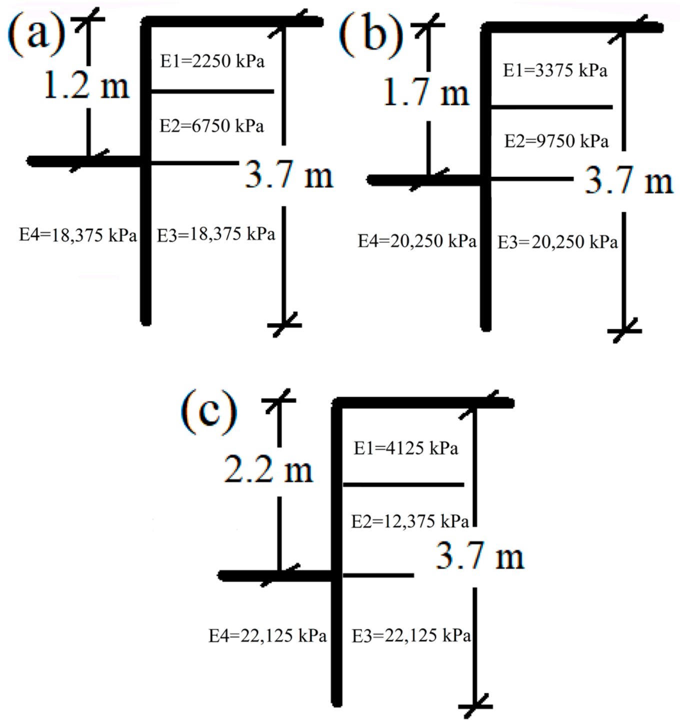

Figure 10. Sketch demonstrating the average soil modulus values at the excavation depths: (**a**) 1.2 m, (**b**) 1.7 m, and (**c**) 2.2 m.

6. The twelfth column contains the surcharge load. It is zero in this case.
7. The thirteenth, fourteenth, fifteenth, and sixteenth columns contain the internal friction angles directly reported by Li and Lehane [22].
8. The seventieth column provides the flexural rigidity of the contiguous pile group per 1 m width. For this calculation, a pile diameter of 0.225 m, an average spacing of 0.4 m, and a modulus of elasticity of 30,000,000 kPa are assumed for the piles. The flexural rigidity (EI) is calculated as 0.225 $m^4/64 \times 1$ m/0.4 m $\times$ 30,000,000 kPa = 9435 kN·m^2.
9. The displacement estimations of the formula for the wall-top and wall-bottom locations are presented in the eightieth and ninetieth columns, respectively. In cases where the actual wall height is different than the nominal wall heights (1, 2, 3, 4, 5, 6, 7, and 8 m), the displacement is calculated by means of interpolation:

$$disp_{H_a} = \frac{\left(disp_{H_{lower}}.\left({H_a}/{H_{lower}}\right) + disp_{upper}.\left({H_a}/{H_{upper}}\right)\right)}{2} \quad (4)$$

where $disp_{H_a}$ is the wall-top or wall-bottom displacement at the actual wall height, H_{lower} is the nearest smaller wall height, H_{upper} is the nearest greater wall height, and $disp_{H_{lower}}$ and $disp_{H_{upper}}$ are the displacements calculated by Equation (4) for H_{lower} and H_{upper}, respectively.

10. The average rotation (rot) is calculated using interpolated displacements and actual wall height with the following formula:

$$rot = (disp_{H_a@wall-top} - disp_{H_a@wall-bottom})/H_a \quad (5)$$

11. Figure 11 includes the wall displacements from two different sources: the test by Li and Lehane [22] and the formula. The displacement plots from both sources exhibit close agreement, indicating that the formula performs reasonably well in estimating wall displacements.

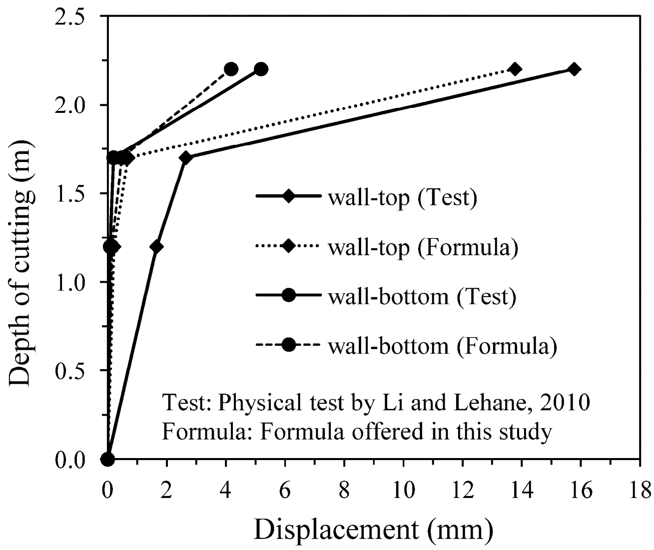

Figure 11. The plots of wall displacements from the site test (Li and Lehane [22]) and the formula (this study).

3.2. Application of the Formula to the Laboratory Test by Bica and Clayton [23]

Bica and Clayton [23] conducted an experimental study using a test tank with dimensions of 1.22 m in length, 0.33 m in width, and 0.47 m in depth. The objective of the study was to investigate the displacement and pressure distribution on a cantilever embedded wall, as depicted in Figure 12. The embedded wall, made of steel, had a thickness of 0.04 m and a width of 0.33 m. It was embedded 0.35 m into dense sand with a unit weight of 15.7 kN/m^3 and an internal friction angle of 47°. To simulate the weight of the sand on the retained side, an equivalent surcharge load was applied. Horizontal and vertical point loads were also applied at 1/3 of the equivalent wall height H to simulate lateral earth pressure and soil–wall friction. Pressure distributions along the embedded part and wall displacements were measured. The simulated wall heights for the test were set at 0.83 m, 1 m, and 1.17 m by adjusting the surcharge and point loads.

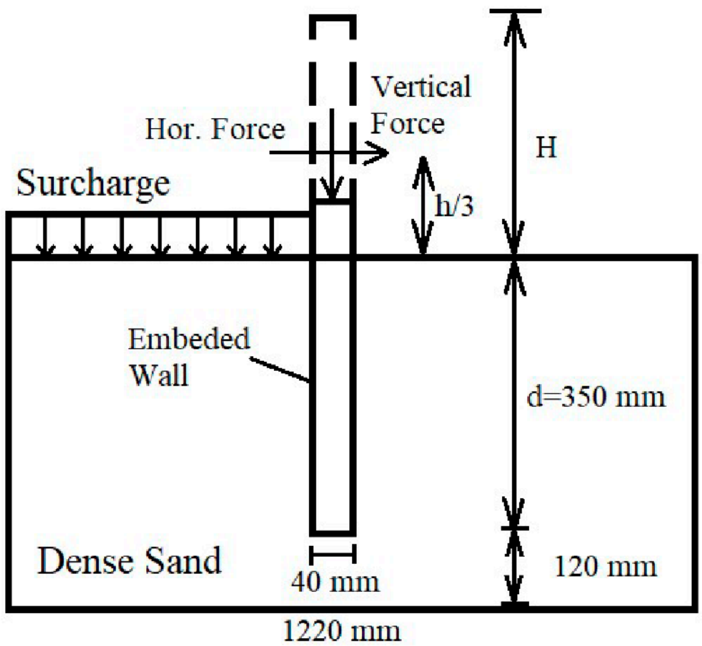

Figure 12. The general setup of the laboratory test by Bica and Clayton [23].

The wall displacement formula corresponding to a wall height of "1 m" is applicable to the test conducted by Bica and Clayton [23]. The unit weight (γ) and internal soil friction (φ) values were set to the same values reported by Bica and Clayton [23] (Table 6). Since there was no additional surcharge load, the "L" value was set to zero. The soil modulus value (E) was not reported in the reference study; hence, it was assumed to be between 5 and 10 MPa. This range is reasonable considering that the E value increases with confining stress, and the total simulated sand depth does not exceed 1.5 m.

Table 6. The input parameters of formula used to predict the displacement measured by Bica and Clayton [23].

H (m)	d (m)	$\gamma_1 = \gamma_2 = \gamma_3 = \gamma_4$ (kN/m^3)	$E_1 = E_2 = E_3 = E_4$ (MPa)	L (kPa)	$\phi_1 = \phi_2 = \phi_3 = \phi_4$ (°)	EI (kN·m^2)
1	0.25–0.49	15.7	5–10	0	47	13,440

Figure 13 illustrates the rotation of the wall relative to the normalized embedment depth. The values provided by the formula align well with those obtained from the test reported by Bica and Clayton [23], indicating agreement between the two sources.

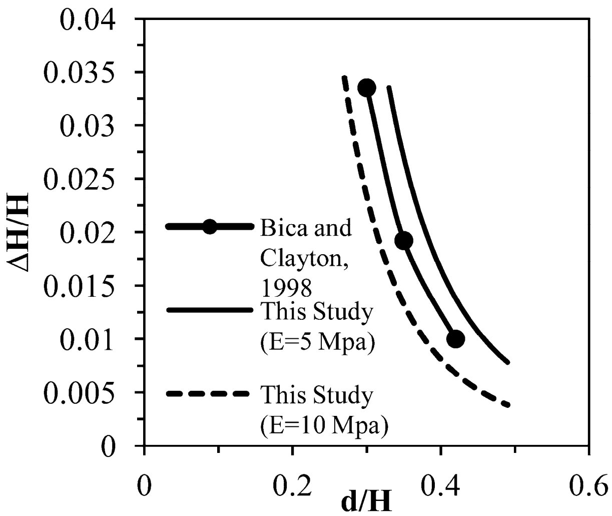

Figure 13. ΔH/H with respect to d/H from the test by Bica and Clayton [23] and the offered formula.

3.3. Influence Coefficients of Input Parameters

The exponent "a" in the expression y = x^a represents the type of relationship between y and x. A value close to 1 for "a" indicates a linear relationship, while values smaller or larger than 1 indicate a non-linear relationship. If "a" is greater than 0, y increases as x increases, and, if "a" is smaller than 0, y decreases as x increases. In essence, "a" can be considered as an influence coefficient (I) that signifies the type and strength of the relationship between y and x.

However, in Equation (3), there are multiple exponents involved, making it impractical to directly use a single exponent as an influence coefficient. In Equation (3), $disp_{wall-top}$ is a function of various variables such as d, γ_1, γ_2, γ_3, γ_4, E_1, E_2, E_3, E_4, ϕ_1, ϕ_2, ϕ_3, ϕ_4, and EI. To determine the influence coefficient between $disp_{wall-top}$ and d, for example, $disp_{wall-top}$ is calculated for different values of d while keeping other variables constant. It is desirable to obtain influence coefficients around 1, so the values of d and $disp_{wall-top}$ are normalized using their respective median values. For d values ranging from 1.6 to 6.4 m, the median d value is set to 4 m. The normalized values of $disp_{wall-top}$ and d are plotted in Figure 14. In this case, the calculated influence coefficient "a" is −3.828.

Table 7 displays the median values of the input parameters. It should be emphasized that the calculation of influence coefficients is specific to walls with a height of 4 m and an embedment depth of 4 m. The values presented in Table 7 represent the medians of the corresponding parameters used in the calculation.

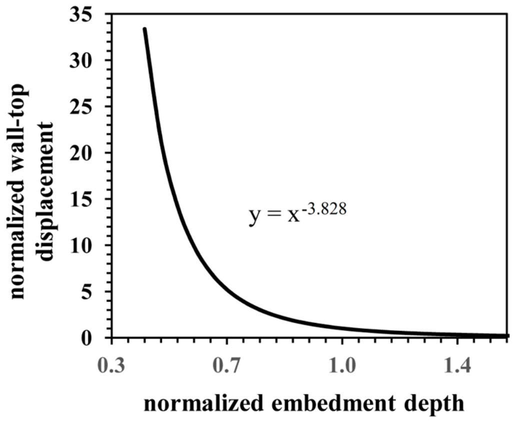

Figure 14. The plot of norm. embedment depth vs. norm. wall-top displacement.

Table 7. The median values for the calculation of the influence coefficients.

H	d	γ_1 (kN/m^3)	γ_2 (kN/m^3)	γ_3 (kN/m^3)	γ_4 (kN/m^3)	E_1 (kPa)	E_2 (kPa)
4	4	20	20	20	20	50,000	50,000
E_3 (kPa)	E_4 (kPa)	L (kN/m)	ϕ_1	ϕ_2	ϕ_3	ϕ_4	EI (kNm^2)
50,000	50,000	0	35	35	35	35	2,500,000

The influence coefficients of d, γ_1, γ_2, γ_3, γ_4, E_1, E_2, E_3, E_4, ϕ_1, ϕ_2, ϕ_3, ϕ_4, and EI can be calculated in a similar way. The influence coefficients (ICs) on wall displacements are summarized in Figure 15. Among the few parameters that can be controlled in a cantilever wall design, the embedment depth plays a pivotal role in wall-top displacement (WTD) with an influence coefficient of $|I_d| = 3.82$. The IC of the soil friction angle on WTD at Zone 2 ranks second with an IC of $|I_{\phi 2}| = 2.29$. The IC of the soil friction angle at Zone 1 is smaller than that of Zone 2 with an IC of $|I_{\phi 1}| = 1.22$. This difference is attributed to the fact that a larger portion of the potential slip line passes through Zone 2. The IC of the soil friction angle at Zone 3 ($|I_{\phi 3}| = 1.57$) is smaller than that of Zone 2 ($|I_{\phi 2}| = 2.29$) but larger than that of Zone 1 with an IC of $|I_{\phi 1}| = 1.22$. The soil friction angle of the wall-front (Zone 4) has an overall smaller IC compared to the zones located at the wall-back ($|I_{\phi \text{wall-front}}| = |I_{\phi 4}| = 1.81 < |I_{\phi \text{wall-back}}| = |I_{\phi 1}| + |I_{\phi 2}| + |I_{\phi 3}| = 5.08$). In other words, the strength of the retained soil is more critical than that of the retaining soil in cantilever walls.

Among the soil unit weights, the IC of the soil unit weight at Zone 1 has the greatest influence on wall displacement with an IC of $|I_{\gamma 1}| = 1.44$. This is due to the fact that Zone 1 has a greater moment arm. Similarly, the soil unit weight at Zone 2 has a positive but comparatively smaller influence on wall displacement with an IC of $|I_{\gamma 2}| = 0.32$. On the other hand, the soil unit weight at Zone 3 and Zone 4 has a negative influence on wall displacement with ICs of $|I_{\gamma 3}| = 0.30$ and $|I_{\gamma 4}| = 0.83$, respectively. This means that the soils located above the excavation level have a positive effect on wall displacement, while the zones below that level have an opposite effect.

The IC of soil modulus on wall displacement is quite small for Zone 1 and 2 with ICs of $-|I_{E1}| = 0.01$ and $|I_{E2}| = 0.03$, respectively. The same ICs for Zone 3 and 4 are $|I_{E3}| = 0.28$ and $|I_{E4}| = 0.65$, respectively. This indicates that the soil modulus of the embedded sides of the wall (Zone 3 and Zone 4) is critical for wall displacement.

The IC of the line load is $|I_{LL}| = 0.10$ and it has positive influence on wall displacement. The flexural rigidity of the wall has a comparatively small influence on wall displacement with an IC of $|I_{EI}| = 0.15$. This implies that designing a thicker wall is not very effective in reducing wall displacement. When the displacement criterion is not satisfied, additional support such as anchors, soil nails, or struts must be considered. In summary, all parameters have an adverse influence on wall-top displacement except for the soil unit weight at the upper backside of the wall and the line load (Zone 1 and Zone 2, Figure 15).

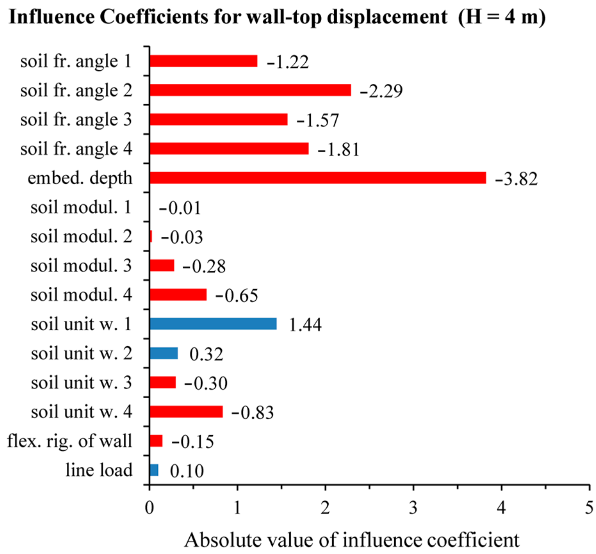

Figure 15. Influence coefficients of the wall in 4 m height and 4 m embedment depth.

3.4. Feasibility of Cantilever Walls with Large Heights

In this study, horizontal displacement formulae have been proposed for wall heights ranging from 1 to 8 m. The baseline configurations for each wall height, along with the relative wall rotation (WR), are presented in Table 8. It is important to note that the internal friction angle for the baseline configurations is set to 35 degrees, which corresponds to the internal friction angle of medium sand. According to the recommendations in Eurocode 7 [30], Annex H, a wall rotation (WR) of 0.002 is considered acceptable for many structures. By referring to Table 8, it can be observed that the WR values for wall heights between 1 and 6 m are safely below the maximum recommended value (MRV) of 0.002. However, for wall heights exceeding 6 m, the WR abruptly increases and approaches the MRV of 0.002. This implies that designing cantilever walls higher than 6 m requires extra caution. For walls higher than 6 m, it is crucial to have sufficiently firm soil present around the wall and ensure that the wall rotation remains significantly lower than the recommended limit. Therefore, careful consideration and additional measures may be necessary when designing and constructing cantilever walls higher than 6 m.

Table 8. Baseline configurations of the walls and the corresponding wall rotations.

No	H (m)	d (m)	γ_1 (kN/m^3)	γ_2 (kN/m^3)	γ_3 (kN/m^3)	γ_4 (kN/m^3)	E_1 ($\times 10^3$ kPa)	E_2 ($\times 10^3$ kPa)	E_3 ($\times 10^3$ kPa)	E_4 ($\times 10^3$ kPa)
1	1	1	20	20	20	20	50	50	50	50
2	2	2	20	20	20	20	50	50	50	50
3	3	3	20	20	20	20	50	50	50	50
4	4	4	20	20	20	20	50	50	50	50
5	5	5	20	20	20	20	50	50	50	50
6	6	6	20	20	20	20	50	50	50	50
7	7	7	20	20	20	20	50	50	50	50
8	8	8	20	20	20	20	50	50	50	50

No	L (kPa)	ϕ_1 (o)	ϕ_2 (o)	ϕ_3 (o)	ϕ_4 (o)	EI (kN·m^2)	$disp_{\text{wall-top}}$	$disp_{\text{wall-bottom}}$	Relative Wall Rotation
1	0	35	35	35	35	2,500,000	0.0002	0.0002	0.0001
2	0	35	35	35	35	2,500,000	0.0013	0.0008	0.0003
3	0	35	35	35	35	2,500,000	0.0032	0.0017	0.0005
4	0	35	35	35	35	2,500,000	0.0058	0.0032	0.0007
5	0	35	35	35	35	2,500,000	0.0087	0.0047	0.0008
6	0	35	35	35	35	2,500,000	0.0133	0.0064	0.0012
7	0	35	35	35	35	2,500,000	0.0223	0.0096	0.0018
8	0	35	35	35	35	2,500,000	0.0314	0.0124	0.0024

3.5. The Horizontal Earth Pressure Distribution and the Displacement of a Typical 3 m-High Wall

The horizontal earth pressure distribution obtained from one of the FE model combinations (H = 3 m, d = 2.0 m, $\gamma_1 = \gamma_2 = \gamma_3 = \gamma_4 = 20$ kN/m^3, $\phi_1 = \phi_2 = \phi_3 = \phi_4 = 35°$, L = 0, $E_1 = E_2 = E_3 = E_4 = 50{,}000$ kPa, $EI = 2.5 \times 10^6$ kN·m^2, and 1 m-thick reinforced concrete wall) has been compared with those of the distributions offered by formulae in the literature (Figure 16). Figure 16 depicts the wall displacement obtained from the finite element (FE) model, represented by a red line. The plot of wall displacement demonstrates a predominantly linear behavior, indicating a rigid response. The maximum displacement observed for the 3 m-high wall is approximately 0.012 m. Notably, at a depth of 1.6 m, the wall solely undergoes rotation without any horizontal displacement. This specific depth serves as the rotational point for analysis purposes. In the soil retained by the wall, extending to the rotational point depth, the horizontal earth pressure distribution (σ_x) obtained from the FE model exhibits a linear pattern. The σ_x values determined using the active earth pressure coefficients proposed by Coulomb's approach (Poncelet [31] and Hamderi [28]) are also illustrated in Figure 16. Remarkably, both formulae yield identical pressure distributions with the FE model up to the depth of the rotational point. However, below the rotational point depth, the pressure distribution provided by the FE model undergoes an abrupt change. At this region, the active pressure is gradually replaced by the passive pressure. On the resisting side of the wall, the FE model presents a parabola-like distribution of horizontal passive pressure above the rotational point depth. Hamderi [28] has developed a formula that calculates the weighted average of the passive earth pressure, taking into account various parameters including the wall rotation and soil modulus. The calculated passive horizontal earth pressure using Hamderi's formula, along with the Coulomb-passive formula, are also included in Figure 16 for comparison. It is worth noting that the Coulomb-passive formula considers the ultimate state, leading to significant deviations from the FE results. As a result, in practical applications, the Coulomb results are often divided by a safety factor. On the other hand, the distribution offered by Hamderi [28] exhibits better accuracy due to its ability to incorporate the actual wall rotation as an input parameter. For further details on the calculations and formulae, refer to Section S5.

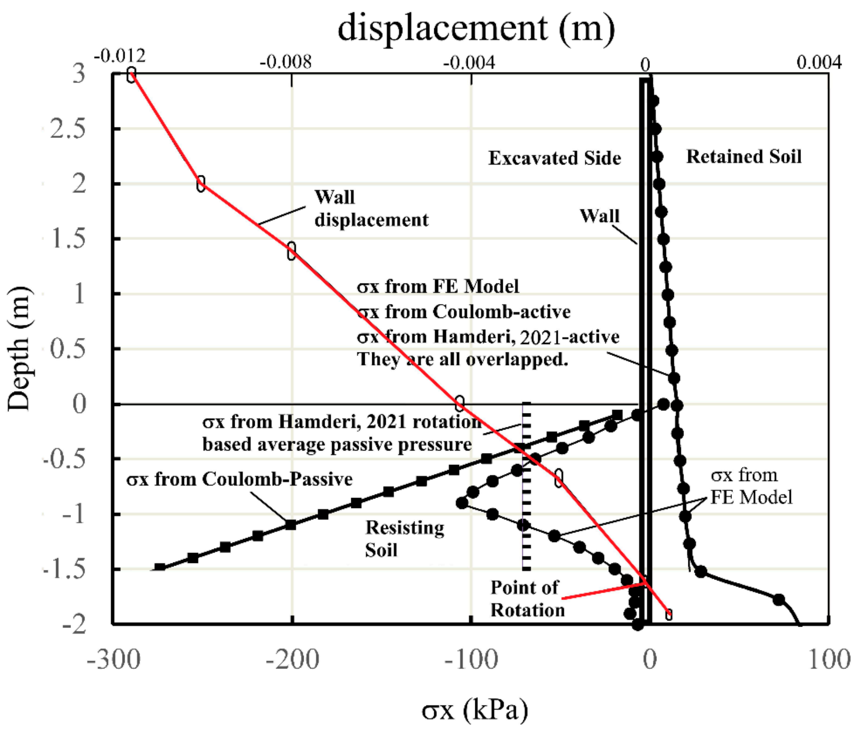

Figure 16. The horizontal earth pressure distributions from different sources: FE-Model, Coulomb-active, Coulomb-passive, and Hamderi [28] active and passive earth pressures.

4. Conclusions

This study proposes formulae for the estimation of wall displacements during the excavation of free embedded cantilever walls. The formulae are based on finite element analyses considering factors such as the wall height, embedded depth, soil moduli, soil internal friction angle, surcharge load, soil weight, and wall modulus.

Several key points can be highlighted:

- The FE model, which was used in the formula derivation, was validated against a physical laboratory study. The comparison of the displacement results demonstrates that the FE model, utilizing Mohr–Coulomb soil properties, effectively simulates the behavior of free embedded cantilever walls.
- The formulae address a range of wall heights from 1 to 8 m.
- Influence coefficients are introduced to indicate the relationship between specific input parameters and wall displacement. The internal friction angle at the back of the wall is identified as the most influential parameter on wall displacement ($|I_{\phi 1}| + |I_{\phi 2}| + |I_{\phi 3}| = 5.08$). The embedment depth ranks as the second most influential parameter ($|I_d| = 3.82$). The internal friction angle at the front of the wall has relatively less influence ($|I_{\phi 4}| = 1.81$). The soil unit weights at the retained side of the wall has a positive influence on wall displacement (($|I_{\gamma 1}| + |I_{\gamma 2}| = 1.76$), while the embedded lower sides of the wall exhibit the opposite effect ($|I_{\gamma 3}| + |I_{\gamma 4}| = 1.13$). The soil modulus at the front side of the wall exerts more influence on wall displacement compared to the backside ($|I_{E4}| = 0.65$ (frontside), $|I_{E1}| + |I_{E2}| + |I_{E3}| = 0.32$ (backside)). Finally, the flexural rigidity of the wall is found to be the least influential input parameter on wall displacement ($|I_{EI}| = 0.15$). In other words, increasing the thickness of the wall is unlikely to significantly reduce wall displacement.
- The proposed formulae are recommended for facilitating swift and reasonably precise computations of cantilever wall displacements. By utilizing these formulae prior to proceeding with an anchored wall, designers can promptly assess the potential for wall stabilization without the need for anchors. It is important to note that anchoring procedures typically require a significant time investment. In summary, the introduced formulae offer a valuable resource for estimating displacements of cantilever walls and can enhance the design workflow for freely embedded structures.

Supplementary Materials: The following supporting information can be downloaded at: https://www.mdpi.com/article/10.3390/app14072802/s1, Section S1: The procedure followed in the generation of 431 wall configurations; Section S2: The mesh and geometry of model walls in MIDAS GTS NX; Section S3: Mesh Convergence Optimization; Section S4: The derivation details of the formulas; Section S5: The horizontal earth pressure distribution and the displacement of a typical 3 m-high wall.

Funding: This research received no external funding.

Institutional Review Board Statement: Not applicable.

Informed Consent Statement: Not applicable.

Data Availability Statement: Some or all data, models, or code generated or used during the study are proprietary or confidential in nature and may only be provided with restrictions (output files of Midas GTS NX runs).

Conflicts of Interest: The authors declare no conflict of interest.

References

1. Krey, H. *Erddruck, Erdwiderstand und Tragfähigkeit des Baugrundes*, 4th ed.; Berlin, W., Ed.; Ernst & Sohn: Berlin, Germany, 1932.
2. Blum, H. *Einspannungsuerhultnisse bei Bohlwerken*, Berlin, W., Ed.; Ernst & Sohn: Hoboken, NJ, USA, 1931.
3. Rowe, P.W. Cantilever sheet piling in cohesionless soil. *Engineering* **1951**, *172*, 316–391.
4. Brinch Hansen, J. *Earth Pressure Calculation*; Danish Technical Press: Copenhagen, Denmark, 1953.

5. Padfield, C.J.; Mair, R.J. *Design of Retaining Walls Embedded in Stiff Clays*; Report 104; Construction Industry Research and Information Association: London, UK, 1984.
6. Yuan, J.X.; Yuwen, Y.; Tham, L.G.; Lee, P.K.K.; Tsui, Y. New approach to limit equilibrium and reliability analysis of soil nailed walls. *Int. J. Geomech.* **2003**, *3*, 145–151. [CrossRef]
7. Nandi, R.; Choudhury, D. Seismic analysis and design of embedded cantilever retaining wall considering non-linear earth pressure distribution effect. In *Earthquake Geotechnical Engineering for Protection and Development of Environment and Constructions*; CRC Press: Boca Raton, FL, USA, 2019; pp. 4103–4110.
8. Peck, R.B. Deep excavations and tunneling in soft ground. In Proceedings of the 7th International Conference on Soil Mechanics and Foundation Engineering (Mexico), Mexico City, Mexico, 25–29 August 1969; pp. 225–281.
9. Clough, G.W.; O'Rourke, T.D. Construction induced movements of insitu walls. In *ASCE Specialty Conference, ASCE Special Publication 25*; ASCE: Reston, VA, USA, 1990.
10. Long, M. Database for retaining wall and ground movements due to deep excavations. *J. Geotech. Geoenviron. Eng.* **2001**, *127*, 203–224. [CrossRef]
11. Conte, E.; Troncone, A.; Vena, M. A method for the design of embedded cantilever retaining walls under static and seismic loading. *Géotechnique* **2017**, *67*, 1081–1089. [CrossRef]
12. Nandi, R.; Choudhury, D. Seismic Analysis of Reinforced Soil Wall Considering Oblique Pull-out of Reinforcements: A Review. *Geotech. Eng.* **2018**, *49*, 90–98.
13. Singh, A.P.; Chatterjee, K. A displacement based approach for seismic analysis and design of cantilever sheet pile walls under surcharge loading. *Comput. Geotech.* **2021**, *140*, 104481. [CrossRef]
14. Kaveh, A.; Behnam, A.F. Charged System Search Algorithm for the Optimum Cost Design of Reinforced Concrete Cantilever Retaining Walls. *Arab. J. Sci. Eng.* **2013**, *38*, 563–570. [CrossRef]
15. Razeghi, H.R.; Nakhaee, M.; Ghareh, S. Effect of Geometrical Properties on Mechanical Behavior of Cantilever Pile Walls (CPW): Centrifuge Tests. *Int. J. Civ. Eng.* **2021**, *19*, 1251–1267. [CrossRef]
16. Phutthananon, C.; Jonpradist, P.; Sirirak, D.; Lueprasert, P.; Jamsawang, P. Improved prediction of pile bending moment and deflection due to adjacent braced excavation. *Front. Struct. Civ. Eng.* **2023**, *17*, 1739–1759. [CrossRef]
17. Diao, Y.; Guo, Y.; Jia, Z.; Zheng, G.; Pan, W.; Shang, D. A simplified method for investigating the bending behavior of piles supporting embankments on soft ground. *Front. Struct. Civ. Eng.* **2023**, *17*, 1021–1032. [CrossRef]
18. Zhang, J.; Shamoto, Y.; Tokimatsu, K. Seismic earth pressure theory for retaining walls under any lateral displacement. *Soils Found.* **1998**, *38*, 143–163. [CrossRef] [PubMed]
19. Nandi, R.; Choudhury, D. Displacement-controlled approach for the analysis of embedded cantilever retaining walls with a distanced strip surcharge. *Comput. Geotech.* **2022**, *151*, 104970. [CrossRef]
20. Chavda, J.T.; Solanki, C.H.; Desai, A.K. Lateral response of contiguous pile wall subjected to staged excavation: Physical and numerical investigations. *Indian Geotech J.* **2017**, *49*, 90–99. [CrossRef]
21. Basha, A.M.; Zakaria, M.H.; El-Nimr, M.T.; Abo-Raya, M.M. Performance Analysis of Axially Loaded Secant Pile Wall Embedded in Sand: An Experimental Investigation. *Arab. J. Sci. Eng.* **2023**, *48*, 13005–13029. [CrossRef]
22. Li, A.Z.; Lehane, B.M. Embedded cantilever retaining walls in sand. *Géotechnique* **2010**, *60*, 813–823. [CrossRef]
23. Bica, A.V.D.; Clayton, C.R.I. An experimental study of the behaviour of embedded lengths of cantilever walls. *Géotechnique* **1998**, *48*, 731–745. [CrossRef]
24. Janbu, N. Soil compressibility as determined by oedometer and triaxial tests. In *Proceedings of the European Conference on Soil Mechanics and Foundation Engineering, Wiesbaden, Germany, 1963*; Deutsche Gesellschaft für Erd-und Grundbau e.V.: Hamburg, Germany, 1963; pp. 19–25.
25. Duncan, J.M.; Chang, C.M. Nonlinear analysis of stress and strain in soils. *J. Soil Mech. Found. Div.* **1970**, *96*, 1629–1653. [CrossRef]
26. Hamderi, M. Comprehensive group pile settlement formula based on 3D finite element analyses. *Soils Found.* **2018**, *58*, 1–15. [CrossRef]
27. Hamderi, M. New approach to group pile load estimation. *Int. J. Geomech.* **2019**, *19*, 4019013. [CrossRef]
28. Hamderi, M. Finite Element–Based Coefficient of Lateral Earth Pressure for Cohesionless Soil. *Int. J. Geomech.* **2021**, *21*, 4021045. [CrossRef]
29. Bowles, J.E. *Foundation Analysis and Design*, 5th ed.; McGraw-Hill Inc.: New York, NY, USA, 1997.
30. Eurocode 7, 2004, EN 1997-1: Geotechnical Design—Part 1: General Rules [Authority: The European Union Per Regulation 305/2011, Directive 98/34/EC, Directive 2004/18/EC]. Available online: https://standards.iteh.ai/catalog/standards/cen/5df964dd-bc1e-4649-bd10-a19881574305/en-1997-1-2004 (accessed on 1 March 2024).
31. Poncelet, J.V. *Mémoire sur la Stabilité des Revêtements et de Leurs Fondations. Note Additionelle sur Les Relations Analytiques qui Lient Entre Elles la Poussée et la Butée de la Terre. Mémorial de L'offi cier du Genie*; Imprimerie et libraire de Bachelier: Paris, France, 1840.